The Application of the Extended Isogeometric Analysis (XIGA) with K-Refinement Approach for the Prediction of Fatigue Life in Linear Elastic Fracture Mechanic

Ata Fardaghaie1, Shahram Shahrooi2, *
Department of Mechanical Engineering, Ahvaz Branch,
Islamic Azad University, Ahvaz, Iran
E-mail: a.aghaie@iauahvaz.ac.ir, shahramshahrooi@iauahvaz.ac.ir
*Corresponding author

Mohammad Shishehsaz3
Department of Mechanical Engineering, Faculty of Engineering,
Shahid Chamran University of Ahvaz, Ahvaz, Iran
E-mail: mshishehsaz@scu.ac.ir

Received: 1 April 2021, Revised: 13 August 2021, Accepted: 14 August 2021

Abstract: This study investigates the fatigue life of a cracked plate subjected to cyclic load under linear elastic fracture mechanics, using a numerical method of extended isogeometric analysis (XIGA) with a K-refinement approach. XIGA is applied to simulate discontinuity problems without meshing and without the necessity for element boundaries to be aligned to crack faces. In this method, the crack faces are simulated by discontinuous Heaviside functions, whereas the singularity in the stress field at the crack tip is simulated by crack tip enrichment functions. The stress intensity factors for the cracks are numerically calculated using the interaction integral method. Paris law of fatigue crack growth is utilized for predicting the fatigue life of a cracked plate. In the standard finite element analysis, there is no refinement method similar to k-refinement. The effect of the k-refinement on the accuracy of the values stress intensity factor and fatigue life is investigated. To achieve this, the order of Non-uniform rational B-Splines (NURBS) basic function is considered as linear, quadratic, and cubic. It is observed that as NURBS orders are increased in k-refinement, results are improved, and the error is lower compared with the analytical solution. The results show that values of stress intensity factor and fatigue life obtained using XIGA are more accurate compared to those obtained by the finite element method. In addition, and they are closer to the results of the analytical solution, and the XIGA method is more efficient.

Keywords: Crack Growth, Extended Isogeometric Analysis, Fatigue Life, K-Refinement, NURBS

How to cite this paper: Ata Fardaghaie, Shahram Shahrooi, and Mohammad Shishehsaz, "The Application of the Extended Isogeometric Analysis (XIGA) with K-Refinement Approach for the Prediction of Fatigue Life in Linear Elastic Fracture Mechanic" , Int J of Advanced Design and Manufacturing Technology, Vol. 15/No. 1, 2022, pp. 29–50. DOI: 10.30495/admt.2021.1927025.1271.

Biographical notes: Ata Fardaghaie is a PhD student at the Department of Mechanical Engineering, Islamic Azad University, Ahvaz, Iran. He received his MSc in Mechanical Engineering from the Islamic Azad University, Dezful branch, Iran, in 2015. His current research interest includes numerical methods in fracture mechanic. **Shahram Shahrooi** received his PhD in Mechanical Engineering from the University of Malaya, Malaysia, in 2010. **Mohammad Shishehsaz** received his PhD in Mechanical Engineering from Northeastern University, USA, in 1985.

1 INTRODUCTION

Investigation of crack propagation through numerical analysis is a significant challenge in the field of linear elastic fracture mechanics. Because of the singularity of the stress at the crack tip, certain elements must be used, which significantly slows down the analysis process. Also, it requires modifying a mesh to improve element boundaries to be aligned to crack faces. To model the cracked problem–precisely, a number of numerical methods such as Finite Element Method (FEM) [1], boundary element methods [2], Extended Finite Element Method (XFEM) [3-5] and element free method [6-7], have been developed in the past years. These methods were developed to reduce the computational cost of mesh generation and remeshing steps and enable these methods to handle crack propagation and discontinuous problems with nonconforming meshes and elements.

In recent years, a powerful numerical method called isogeometric analysis (IGA) [8] is used to analyze engineering problems which has been presented. This method is based on mathematical computational processes in modeling computer-aided design (CAD). In fact, the basic functions used to create geometry in CAD are used to estimate the analysis. This approach has been presented to overcome the difficulties of crack geometric topological changes and remeshing during crack propagation, such as combinative methods for crack modeling and analyzing. For example, the B-spline or NURBS are employed for defining the geometry as well as the approximate solution. The exact model is preserved, and the remeshing is performed without any further communication with the initial CAD model. Therefore, there is not a geometric error in the sense that the model is exact. This might be the main advantage of this method. Construction of the mesh itself can be a time-consuming step in the analysis process, and if the purpose is to achieve a precise solution with a set of refinements, the quality of the geometric approximation must also be improved simultaneously to obtain the required precision.

Recently, the IGA was combined with extended finite element (XFEM) to analyze the problems involving discontinuities linear elastic fracture mechanic. This numerical method development is called an extended isogeometric analysis (XIGA). The XFEM [9-11] allows modeling cracks with an incompatible mesh through the introduction of discontinuous enrichment functions. Using the level set technique and its simultaneous use in XFEM, this method provides a means for propagating cracks without re-meshing [12]; optimal convergence rates are obtained by introducing tip enrichment functions from the asymptotic crack tip displacement field [13].

In order to perform geometric refinement, it is necessary to communicate between analytical geometry and refinement. The important point is that if the meshing encompasses exactly the appropriate geometry of the analysis, the refinement can be done at any stage within the framework of the analysis, and the need to communicate with the geometry of the problem is completely eliminated. One of the most interesting properties of B-spline and NURBS is the variety of techniques in which their basic functions are expanded apart from geometry and its parameters. This makes the basic refinement techniques in the isogeometric analysis lead to further development throughout the refining space. So not only do we dominate the size of elements and order of the basic functions, but also we can control the continuity of the basic functions. This is one of the most important features of the isogeometric numerical method.

In other words, once the initial geometry mesh is constructed, the mesh can incorporate real geometry, and at any stage without problem, geometry with knot insertion, order elevation, and k-refinement techniques will be completely improved. These techniques will be explained further in the following sections. Ghorashi et al. [14] analysed local refinement in XIGA on Fracture analysis using the T-spline basis functions. Jiming et al. [15] investigated fracture behavior of single and multiple cracks in two-dimensional solids by an adaptive XIGA based on locally refined B-splines. They have shown the effectiveness of this method in several examples.

One of the equipments used in the industry is a plate or other 2D structures. All the plates do not have a homogeneous structure during their manufacturing process, and structural defects such as holes and cracks are almost inevitable. The presence of cracks reduces the structural strength, and it causes a fracture. Therefore, it is very important to examine and analyze their fracture behavior. To investigate cracks in plates, several numerical methods such as boundary element methods [16], coupled FEM and EFG method [17-20], and extended finite element method [21-22] have been developed to solve the cracked plate problems. Menouillard and Belytschko [23] have reported that the accuracy of the stress intensity factor can also be developed by combining a meshfree method with the crack tip enrichment. Tanaka et al. [24-25] improved a meshfree method in terms of reproducing kernel particle method to numerically evaluate the moment intensity factor of Mindlin-Reissner plate. Tran et al. [26], used isogeometric analysis for the static, dynamic, and buckling response of plates. Yuan et al. [27], investigated Mode I stress intensity factors for cracked special-shaped shells under bending. Nguyen et al. [28] proposed the Symmetric Galerkin Boundary Element Method (SGBEM) based on the isogeometric method and the basic functions of NURBS, for two dimensional fracture problems. The results of this study showed that

the use of NURBS basic functions instead of Lagrangian functions leads to better accuracy and convergence in the solutions but in general this method has high computational cost due to the solution of dual integrals. Verhoosel et al. [29-30], applied the concept of knot insertion to create a discontinuous displacement field. Hao et al. [31] used an isogeometric method for buckling analysis in variable-stiffness composites. In this type of composite, the discontinuity of the elements due to the variability of the stiffness is reported in the finite element method. Therefore, the isogeometric method is used in buckling analysis of the composite sheet, and the excellent accuracy of the results compared to the finite element method is shown. Tran et al. [32], by combining the XIGA and high-order deformation theory (HSDT) on the plates, developed a new and effective formulation for vibration analysis in cracked FGM plates. Bhardwaj et al. [33-34] used the XIGA to perform fracture analysis of cracked plates under static loading and different boundary conditions. Nguyen et al. [35], used XIGA for the analysis of the thickness cracks in thin-shell structures. The intricacy of the enrichment strategy and the computational costs significantly reduced. Kumar et al. [36], Investigated the crack tip plastic zones by the extended isogeometric analysis by studying the effect of holes on the shape and size of crack tip plastic zones. Considering the literature, it is obvious that no studies has been reported on the investigation of the fatigue life of a cracked plate subjected to cyclic load and also evaluation of the effect of k-refinement on fatigue life. In this research, the extended isogeometric analysis (XIGA) with the k-refinement approach is applied to investigate the fatigue life of a cracked plate subjected to cyclic load. Toward this purpose, the crack faces are simulated by discontinuous Heaviside functions, while the singularity in the stress field at the crack tip is simulated by crack tip enrichment functions. The order of NURBS basic function is taken as linear, quadratic, and cubic to implement K-refinement. In numerical examples, considering the geometry, boundary, and loading condition are used to validate this method.

This paper is organized as follows: In Section 2, the isogeometric analysis is introduced and B-spline and NURBS basic functions, refinement in IGA and formulation of IGA for the 2D problem are defined. In Section 3, Level set method is described and the formulation of extended isogeometric analysis for crack simulation is presented. Section 4 represents the interaction integral method for computing the stress intensity factor. The fatigue crack growth and fatigue life are expressed in Section 5. Section 6 describes various numerical examples for investigation of the stress intensity factor, the fatigue life of the cracked plate and the effect of the K-refinement on them to verify the accuracy of the method. Finally, conclusions are presented in section 7.

2 ISOGEOMETRIC ANALYSIS METHOD

2.1 B-Splines and Non-Uniform Rational B-Splines (NURBS)

The B-spline basic function of orders p is constructed in parametric space using a recursive relation and the assumed knot vector. This means that to produce basic functions with each order, lower order basic functions are needed. One dimensional Knot vector $\Xi = \{\xi_1, \xi_2, \ldots, \xi_{n+p+1}\}$, ($\xi_i \in R$), is a non-decreasing of coordinates in the parametric space, where ξ_i is the i^{th} knot and n shows the number of basic functions of order p. Knots divide the parametric space into knot spans. A knot vector is called open if ξ_1 and ξ_{n+p+1} are repeated $p+1$ time. The use of an open knot vector in isogeometric analysis satisfies the characteristic of the Kronecker Delta at the boundary control points [37]. According to the assumed knot vector, the B-spline basic function of orders p = 0 and higher orders (p > 0) are defined as [38]:

$$N_{i,0} = \begin{cases} 1 & \xi_i \le \xi \le \xi_{i+1} \\ 0 & otherwise \end{cases} \quad \text{for } p = 0 \tag{1}$$

$$N_{i,p}(\xi) = \frac{\xi - \xi_i}{\xi_{i+p-1} - \xi_i} N_{i,p-1}(\xi) + \frac{\xi_{i+p} - \xi}{\xi_{i+p} - \xi_{i+1}} N_{i+1,p-1}(\xi) \quad \text{for } p > 0 \tag{2}$$

Since the derivative of the basic functions is needed in calculations later, the derivatives of the i^{th} basic function can be determined for a given polynomial degree p and knot vector Ξ:

$$\frac{dN_{i,p}(\xi)}{d\xi} = \frac{p}{\xi_{i+p} - \xi_i} N_{i,p-1}(\xi) - \frac{p}{\xi_{i+p+1} - \xi_{i+1}} N_{i+1,p-1}(\xi) \tag{3}$$

The B-spline curve can be evaluated by $N_{i,p}(\xi)$ and control point coordinates set P_i as:

$$c(\xi) = \sum_{i=1}^{n} N_{i,p}(\xi) P_i \tag{4}$$

In the two-dimensional parametric space ξ and η, the B-spline surfaces are derived by tensor multiplying the two knot vectors $\Xi = \{\xi_1, \xi_2, \ldots, \xi_{n+p+1}\}$ and $H = \{\eta_1, \eta_2, \ldots, \eta_{m+q+1}\}$ as follows:

$$s(\xi, \eta) = \sum_{i=1}^{n} \sum_{j=1}^{m} N_{i,p}(\xi) M_{j,q}(\eta) P_{i,j} \tag{5}$$

Where, $N_{i,p}(\xi)$ and $M_{j,q}(\eta)$ are the p_{th} and q_{th} order univariate B-spline basic functions respectively and $P_{i,j}$ form a $n \times m$ set of control net.

B-spline piecewise polynomials generalized to Non-uniform Rational B-Spline (NURBS) basic functions are as follows [38]:

$$R_{i,p}(\xi) = \frac{w_i N_{i,p}(\xi)}{W(\xi)} = \frac{N_{i,p}(\xi) w_i}{\sum_{i=0}^{n} N_{i,p}(\xi) w_i} \quad (6)$$

Where, $N_{i,p}$ is the B-spline basic function of order p, and w_i is the Non-negative weight, corresponding to i_{th} control point. In a procedure analogous to B-spline curves, NURBS curves are created as follows:

$$C(\xi) = \sum_{i=1}^{n} R_{i,p}(\xi) P_i \quad (7)$$

Where, $R_{i,p}(\xi)$ is the NURBS basic function, and P_i is the control point coordinates set.

NURBS surfaces are created by tensor yield of knot vectors $\Xi = \{\xi_1, \xi_2, \dots, \xi_{n+p+1}\}$ and $H = \{\eta_1, \eta_2, \dots, \eta_{m+q+1}\}$ in two dimensional parametric space:

$$S(\xi, \eta) = \sum_{i=1}^{n} \sum_{j=1}^{m} R_{i,j}^{p,q} P_{i,j} \quad (8)$$

Where, $P_{i,j}$ is the ij_{th} control point and $R_{i,j}^{p,q}$, the NURBS basic function in two directions is defined as follows:

$$R_{i,j}^{p,q}(\xi, \eta) = \frac{N_{i,p}(\xi) M_{j,q}(\eta) w_{i,j}}{\sum_{i=0}^{n} \sum_{j=0}^{m} N_{i,p}(\xi) M_{j,q}(\eta) w_{i,j}} \quad (9)$$

Where, $N_{i,p}(\xi)$ and $M_{j,q}(\eta)$ are the i_{th} p and j_{th} q order univariate B-spline basic functions respectively, and $w_{i,j}$ is the Non-negative weight corresponding to ij_{th} control point.

In two dimensional parametric spaces, the patch domain (Ω_{patch}) is defined as follows:

$$\Omega_{patch} = \{(\xi, \eta) | \xi \epsilon [\xi_1, \xi_{n+p+1}], \eta \epsilon [\eta_1, \eta_{m+q+1}]\} \quad (10)$$

And element domain is equal to $\Omega_e = [\xi_i, \xi_{i+1}) \times [\eta_j, \eta_{j+1})$. For each knot span, there are $(p+1) \times (q+1)$ non-zero NURBS basic functions. Since the number of basic functions is equal to the control points, $n_e = (p+1) \times (q+1)$ is the number of control points associated with each knot span.

2.2. Refinement in Isogeometric Analysis Method

As mentioned in the introduction, commonly, three techniques are used to improve the mesh in the isogeometric numerical method. The first technique by which one can increase analysis accuracy is knot insertion. New knots are added to the knots vector without changing a curve from the aspect of geometry and parametric properties. The insertion of new knots values is clearly similar to the h-refinement in the finite element method that divides existing elements into new smaller elements. It is important to note that the numbers of new base functions to be created and their continuity along the boundaries of the element with finite elements is different [39]. The second technique by which one can increase analysis accuracy is order elevation. The process requires elevating the polynomial order of the basic functions.

In this technique, the number of iterations per knot increases, but no new knot is added to the knots vector, and similar to the knot insertion technique, the geometry and curve parameters do not change. Therefore, continuity across element boundaries to order elevation technique is C^0. The order elevation is very similar to the p-refinement in the finite element method, the main difference is that the number of elements does not change while the accuracy of the solution can be improved by increasing the order of the basic functions [39]. Knot insertion and order elevation techniques are the two main refinement techniques of the isogeometric analysis method so that new knots values can be repeated only once and create new elements. It is also possible to duplicate the existing knot value and reduce the continuity of the basic functions along the element boundaries.

In this case, the continuity along the element boundaries will be C^{p-1}. It is also possible to duplicate the existing Knot value and reduce the continuity of the basic functions along the element boundary. This process constructs these techniques better and more flexible than the h-refinement and p-refinement. In the isogeometric analysis method, there is a unique refinement technique called *k*-refinement. In a one knot vector of order p for a value between two knots, the number of continuous derivatives of the basic functions is $p-1$. In k-refinement, if we elevate the order from p to q, only knots at the beginning and the end of the knot vector are repeated, and the other knots will not be repeated. This causes remaining the continuity equal to C^{q-1} over the whole basic function. In k-refinement, there is a homogeneous structure within patches, and growth in the number of control variables is limited [40]. K-refinement has no similar practice in standard finite element analysis.

Figure 1 represents the results of the k-refinement technique with a much smaller number of basic functions, each of which is of C^{p-1} continuity along the element boundaries. According to the above explanation, it could be concluded that this refinement requires fewer control points. Thus, compared to the other two refinements, it reduces the computational cost. In this study, the effect of the k-refinement on the accuracy of the values stress intensity factor and fatigue

life is investigated. To achieve this, the order of NURBS basic function is taken as linear, quadratic, and cubic.

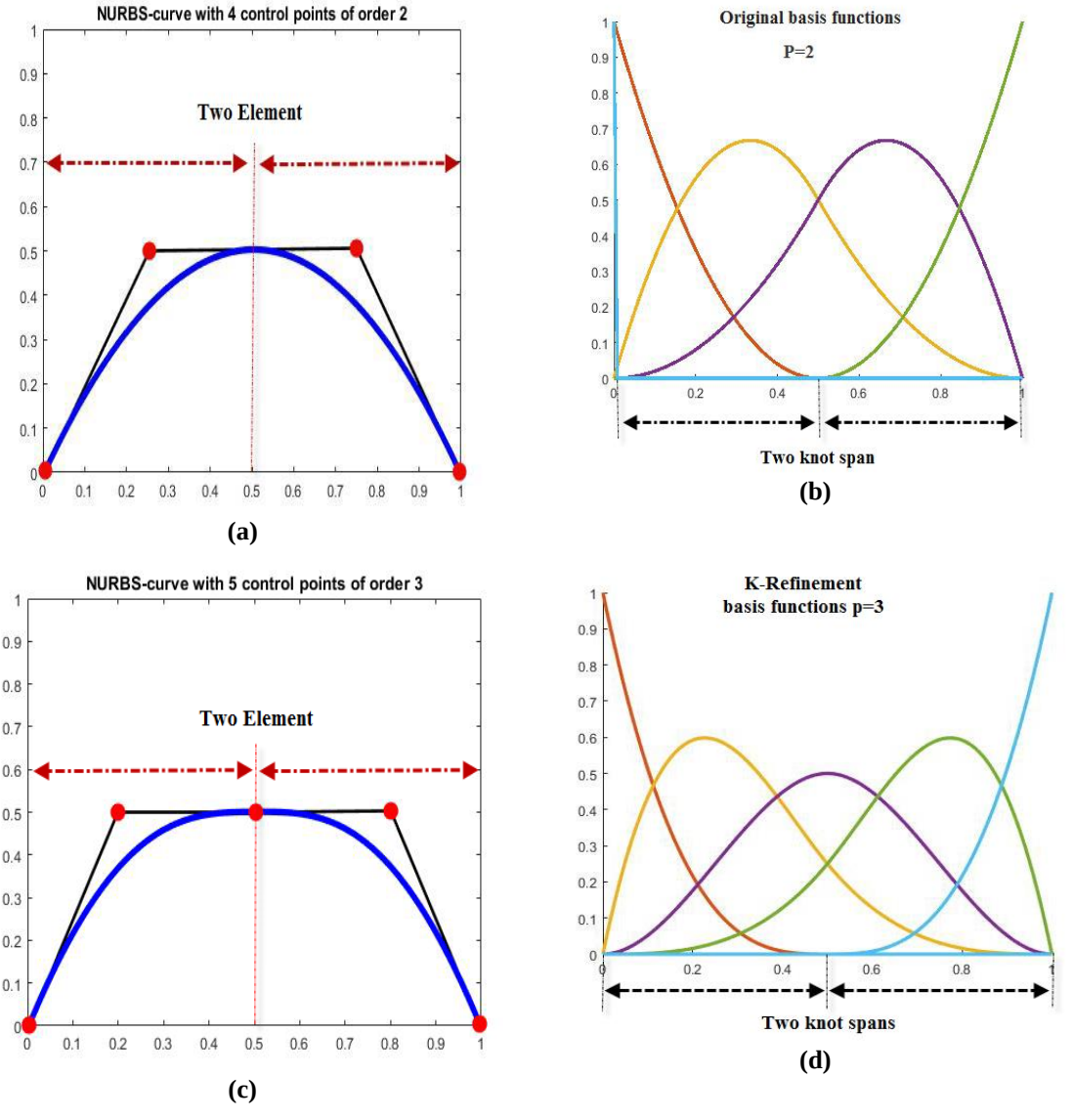

Fig. 1 k-refinement. Original NURBS-curve for knot vector Ξ=[0 0 0 0.5 1 1 1], (b): Original basic function for knot vector Ξ=[0 0 0 0.5 1 1 1], k-refinement NURBS-curve for knot vector Ξ=[0 0 0 **0** 0.5 **1** 1 1 1], (d): k-refinement basic function for knot vector Ξ=[0 0 0 **0** 0.5 **1** 1 1 1] whit continuity C^{p-1}.

2.3. Isogeometric Analysis for 2D Plane Stress Problem

In this numerical method, the discretization is based on the NURBS basic functions. At a particular control point x = (x, y), corresponding to the point ξ = (ξ, η) in the parametric coordinates; hence the geometry and solution space are approximated as follows:

$$\boldsymbol{X}(\xi,\eta) = \boldsymbol{RP} \qquad \xi,\eta \in \Omega_{patch} \tag{11}$$

$$\boldsymbol{u^h}(\xi,\eta) = \boldsymbol{Rd} \qquad \xi,\eta \in \Omega_{patch} \tag{12}$$

We can convert R and P from their matrix-form to vectors by mapping from i, j subscripts to k:

$$k = i + (j-1)n \quad \begin{cases} i = 1,2,\dots,n \\ j = 1,2,\dots,m \end{cases} \tag{13}$$

As seen in the above Equations, with respect to the isoparametric concept, the NURBS basic functions are used to discrete the geometry, as well as the solution

field approximation. The vector of control points in physical space is defined as:

$$\boldsymbol{P} = \{P_{1x} \;\; P_{1y} \;\; \dots \;\; \dots \;\; P_{Nx} \;\; P_{Ny}\}^T \tag{14}$$

Similarly to the values of approximation space at the control points are regulated in the displacement vector:

$$\boldsymbol{d} = \{d_{1x} \;\; d_{1y} \;\; \dots \;\; \dots \;\; d_{Nx} \;\; d_{Ny}\}^T \tag{15}$$

Then the NURBS basic functions R matrix is renovated in the following form:

$$\boldsymbol{R} = \begin{bmatrix} R_1 & 0 & R_2 & 0 & \dots & \dots & R_N & 0 \\ 0 & R_1 & 0 & R_2 & & & 0 & R_N \end{bmatrix} \tag{16}$$

Now stiffness matrix can be obtained as follows for a single patch:

$$K_e = \int_{\Omega_e} \boldsymbol{B}^T D^{2D} \boldsymbol{B} d\Omega \tag{17}$$

Ω_e is the domain of knot span in the parametric space, D^{2D} is the mechanical properties matrix, and B is the strain–displacement matrix which is defined:

$$\boldsymbol{B} = \begin{bmatrix} \frac{\partial R_1}{\partial \mathrm{X}} & 0 & \cdots & \frac{\partial R_{np}}{\partial \mathrm{X}} & 0 \\ 0 & \frac{\partial R_1}{\partial \mathrm{Y}} & & 0 & \frac{\partial R_{np}}{\partial \mathrm{Y}} \\ \frac{\partial R_1}{\partial \mathrm{Y}} & \frac{\partial R_1}{\partial \mathrm{X}} & & \frac{\partial R_1}{\partial \mathrm{Y}} & \frac{\partial R_{np}}{\partial \mathrm{X}} \end{bmatrix} \tag{18}$$

Where:

$$\begin{pmatrix} \frac{\partial R_i}{\partial \mathrm{X}} \\ \frac{\partial R_i}{\partial \mathrm{Y}} \end{pmatrix} = \boldsymbol{J^{-1}} \begin{pmatrix} \frac{\partial R_i}{\partial \xi} \\ \frac{\partial R_i}{\partial \eta} \end{pmatrix} \tag{19}$$

J is the Jacobian matrix, defined as:

$$\mathbf{J} = \begin{bmatrix} \frac{\partial \mathrm{X}}{\partial \xi} & \frac{\partial \mathrm{Y}}{\partial \xi} \\ \frac{\partial \mathrm{X}}{\partial \eta} & \frac{\partial \mathrm{Y}}{\partial \eta} \end{bmatrix} \tag{20}$$

In the presence of body forces $\boldsymbol{b}$ and traction forces $\boldsymbol{t}$, the force vector is defined as:

$$F_e = \int_{\Omega_e} R^T \boldsymbol{b} d\Omega + \int_{\Gamma_{te}} R^T \hat{\boldsymbol{t}} \, d\Gamma \tag{21}$$

Where, Ω and Γ are the domain and traction boundary and R is the NURBS basic function. Finally, the displacement vector d is obtained using the following equilibrium Equation:

$$Kd = F \tag{22}$$

3 FORMULATION OF EXTENDED ISOGEOMETRIC ANALYSIS

3.1. Level Set Method for Selection of Knot Spans for Enrichment

The level set method is used to recognize the crack position in the solution field. In order to apply the level set method in the extended isogeometric analysis, first, Geometry is described by the knot vectors and control points. Then level set values for all control points of knot spans are calculated relative to the crack position. The level set function has two values, normal and tangent level set, which are called N.l.s and T.l.s in this study. The first one explains the crack surface {x: N.l.s(x) = 0 and T.l.s ≤ 0}, and the second is used to explains the crack tip {x: N.l.s(x) = 0 and T.l.s(x) = 0}. Figure 2 shows how to identify the crack position by level set function.

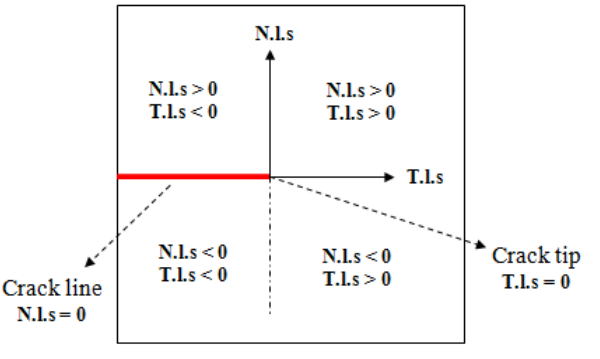

Fig. 2 Illustration of the level set function N.l.s and T.l.s.

If the coordinates of the beginning and end of the crack line are (x_0, y_0) and (x_1, y_1), respectively, the level set values for each control point are given:

$$N.l.s = \frac{(y_0 - y_1)x + (x_1 - x_0)y + (x_0 y_1 - x_1 y_0)}{\sqrt{(x_1 - x_0)^2 + (y_1 - y_0)^2}} \tag{23}$$

$$T.l.s = ([xy] - [x_1 y_1]).\left(\frac{(x_1 - x_0)\vec{i} + (y_1 - y_0)\vec{j}}{|(x_1 - x_0)\vec{i} + (y_1 - y_0)\vec{j}|}\right) \tag{24}$$

With "Eq. (23) and Eq. (24)", the split knot span and the crack tip knot span can be identified. Thus for split knot span:

$$Max(N.l.s) \times Min(N.l.s) < 0 \quad \& \quad Max(T.l.s) < 0 \tag{25}$$

And for crack tip knot span:

$$Max(N.l.s) \times Min(N.l.s) < 0 \quad \& \quad Max(T.l.s) \times Min(T.l.s) < 0 \tag{26}$$

Figure 3 shows the control points associated with the split knot spans and crack tip knot spans identified by the level set method, which should be enriched as described in the following section.

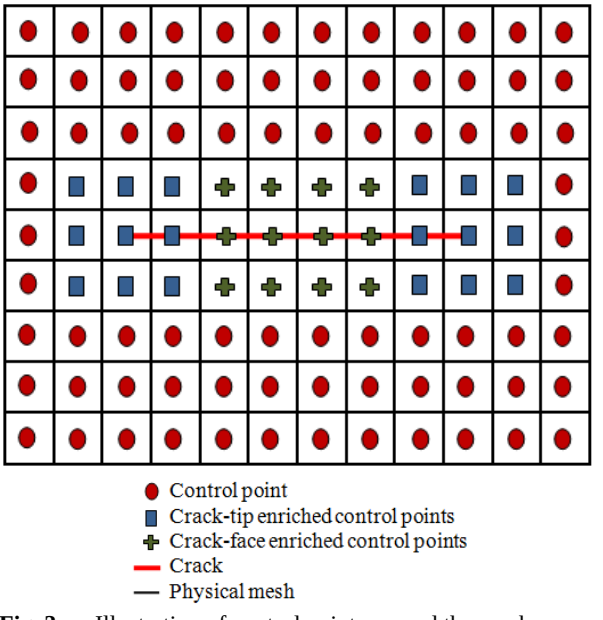

Fig. 3 Illustration of control points around the crack.

3.2. XIGA Approximations for Cracks

Extended isogeometric analysis is a newly developed computational approach that combines the isogeometric analysis method and extended finite element. As a result, a crack can be simulated independently of the mesh and can model the crack growth without the necessity of re-meshing. The basic concept of the extended finite element is based on the expansion of base functions in the solution field by enrichment functions that are capable of modeling the crack discontinuity. To model the cracks in XIGA, the knot span intersected by the discontinuities are identified as enriched knot span. Level set functions are used to identify the enriched and non-enriched knot spans. The knot spans, including the crack faces, are named as split knot span, whiles the knot span, including the crack tips, are named as tip knot span. Each univariate NURBS basic function can be appropriated to its associate control point. Also, it is obvious that each NURBS basic function has its own support domain and its value outside this domain is zero. These aspects are to detect the control points related to the split and tip knot span. The number of control points related to a split or tip knot span depends on the NURBS basic functions order. So in p-refinement and k-refinement, the change in the NURBS basic functions order changes the control points. The control points related to knot span, which are cut off by the crack face, are enriched with Heaviside function, while the control points related to knot span, including the crack tip, are enriched with crack tip enrichment functions. At a particular control point $x_i = (x, y)$, corresponding to the point $\xi = (\xi, \eta)$ in the parametric coordinates, the formulation of extended isogeometric analysis are given [41]:

$$u^{h}(\xi) = u^{IGA}(\xi) + u^{\mathrm{XIGA}}(\xi) = \sum_{i=1}^{n} R_i(\xi) u_i + u^{\mathrm{enrichment}} \tag{27}$$

The first term represents the Conventional isogeometric displacement approximation without the presence of the crack and the additional terms represent the displacement approximation in the presence of a crack. In this case, we need to define two types of enrichments: the Heaviside type enrichment *H(x)* and the tip enrichment functions $S_\alpha(x)$. "Eq. (27)" can be expressed by utilizing the Heaviside functions and crack tip functions as:

$$u(\xi) = \sum_{i=1}^{n_{cp}} R_i(\xi) u_i + \sum_{j=1}^{n_{cf}} R_i(\xi)[H(\xi) - H(\xi_i)]\, a_j + \sum_{k=1}^{n_{ct}} R_k(\xi) \left\{ \sum_{\alpha=1}^{4} [S_\alpha(\xi) - S_\alpha(\xi_i)] b_k^\alpha \right\} \tag{28}$$

Where, $R_i(\xi)$ is the NURBS basic functions; $H(\xi)$ and $S\alpha(\xi)$ are the Heaviside and crack tip enrichment functions, respectively. a_j is the additional DOFs related to modeling discontinuity at the crack face, b_k is the additional DOFs related to modeling discontinuity and singularity at the crack tip. ncf is the number of control points associate with split knot span on a crack face that is enriched with Heaviside function, and nct is the number of control points associate with crack tip knot span in a crack tip that is enriched with crack tip functions. The Heaviside function, which is used for the

enrichment of the control points associated with the crack faces, is defined as follows:

$$H(X) = \begin{Bmatrix} +1 & if\ (X - X^c).n > 0 \\ -1 & otherwise \end{Bmatrix} \quad (29)$$

Where, x is any interest point around the crack and x^c is the nearest point on the crack face as shown in "Fig. 4". If x is above the crack face, the Heaviside function value is +1 otherwise, it is -1; n is normal vectors of the crack alignment at point x.

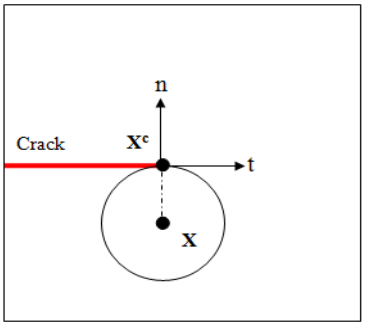

Fig. 4 Heaviside functions for crack face enrichment

The asymptotic near tip displacement field is presented in [42]. It can be shown that the asymptotic near crack tip displacement field can be expressed by the following function $S(x)$, defined in the polar coordinate system:

$$S_\alpha(x) = \left\{\sqrt{r}\cos\frac{\theta}{2}, \sqrt{r}\sin\frac{\theta}{2}, \sqrt{r}\cos\frac{\theta}{2}\sin\theta, \sqrt{r}\sin\frac{\theta}{2}\sin\theta\right\} \quad (30)$$

Where, r and θ denote the polar coordinates of a point with respect to the crack tip, as shown in "Fig. 5".

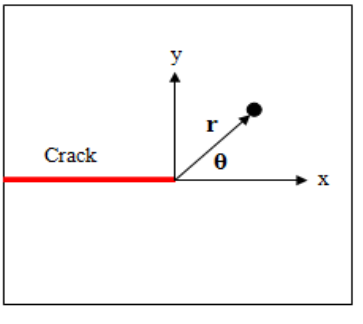

Fig. 5 Polar coordinates of the crack tip.

In the extended isogeometric analysis, the mesh consists of a non-enriched knot span and enriched knot span, including split and tip. Enriched split knot spans are those which are intersected by the discontinuity of crack face, and enriched tip knot spans are those at the tip of the crack. Figure 6 shows NURBS basic functions order 2 and 4 respectively in implementation of XIGA to a cracked plate.

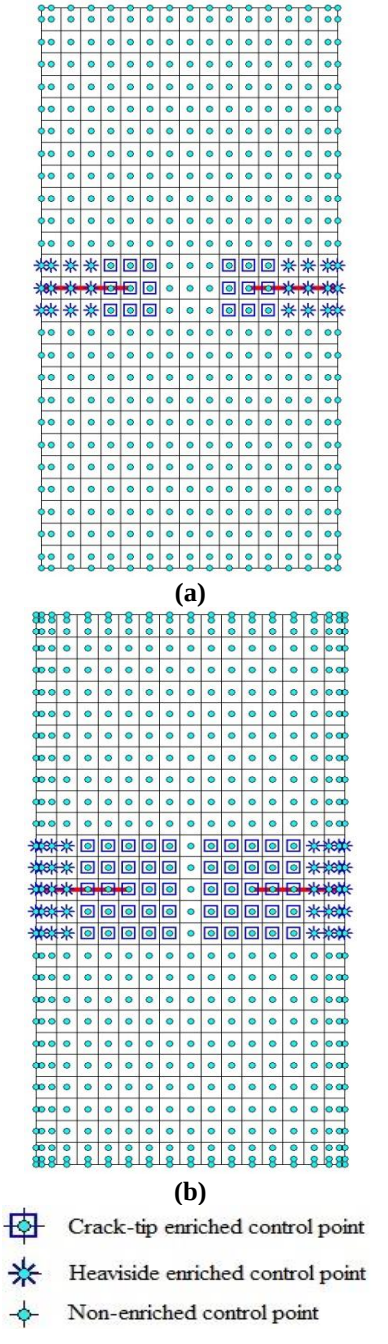

Fig. 6 Implementation of XIGA to cracked plate: (a): NURBS basic functions order 2, and (b): NURBS basic functions order 4.

As shown in "Fig. 1", the number of Knots is changed by implementation of the k-refinement. Therefore basic functions will be changed according to "Eq. (1)" and "Eq. 2". Therefore, based on "Eq. 9", the order of the basic function (p and q) and their continuity change. With the changes made in the Knots and basic functions as shown in "Fig. 6", the number and distribution of control points will change, and with a more appropriate

distribution of control points in the crack zone, the calculation of stress intensity factors will be improved. The main displacement vector in the presence of additional enrichment DOFs in "Eq. (28)" can be written as follows:

$$\mathrm{U} = \{u\ a\ b_1\ b_2\ b_3\ b_4\}^T_{M\times 1} \tag{31}$$

Where, u is the DOFs vector without considering the crack, a is the DOFs vector regarding control points that are enriched with Heaviside functions, and b_i is the DOFs vector regarding control points that are enriched with crack tip enrichment functions, and M represents the total DOFs. In 2D problem:

$$M = 2N + 2m_{split} + 8m_{tip} \tag{32}$$

Where, N is the number of control points, m_{split} is the number of the control point of split knot span, and m_{tip} is the number of the control point of tip knot span. Finally, the control variables can be obtained by solving the following equilibrium Equation:

$$[\mathrm{K}]\{\mathrm{d}\} = \{\mathrm{F}\} \tag{33}$$

Where, K and F are the assembled stiffness matrix and force vector respectively.
In XIGA formulation, the stiffness matrix of knot span is obtained as:

$$K_{ij}^{e} = \begin{bmatrix} K_{ij}^{uu} & K_{ij}^{ua} & K_{ij}^{ub} \\ K_{ij}^{au} & K_{ij}^{aa} & K_{ij}^{ab} \\ K_{ij}^{bu} & K_{ij}^{ba} & K_{ij}^{bb} \end{bmatrix}, \quad \mathrm{i,j} = 1,2,3,\dots,n_{el} \tag{34}$$

Where, n_{el} is the number of knot span and:

$$K_{ij}^{r,s} = \int_{\Omega_e} (B_i^r)^T D^{2D} B_j^s \, d\Omega \tag{35}$$

Where, r, s=u, a, b. It is obvious that for non-enriched knot span $K_{ij}^{e} = K_{ij}^{uu}$. Also, the force vector in XIGA formulation is obtained as:

$$F_i = \left\{F_i^u\ F_i^a\ F_i^{\mathrm{b}_1}\ F_i^{\mathrm{b}_2}\ F_i^{\mathrm{b}_3}\ F_i^{\mathrm{b}_4}\right\}^T \tag{36}$$

$$F_i^u = \int_{\Omega_e} R_i^T \boldsymbol{b} d\Omega + \int_{\Gamma_t} R_i^T \hat{\boldsymbol{t}}\, d\Gamma \tag{37}$$

$$F_i^a = \int_{\Omega_e} R_i^T H \boldsymbol{b} d\Omega + \int_{\Gamma_t} R_i^T H \hat{\boldsymbol{t}}\, d\Gamma \tag{38}$$

$$F_i^{b_\alpha} = \int_{\Omega_e} R_i^T S_\alpha \boldsymbol{b} d\Omega + \int_{\Gamma_t} R_i^T S_\alpha \hat{\boldsymbol{t}}\, d\Gamma \tag{39}$$

Where, R_i the NURBS basic functions. The NURBS basic function derivatives for forming the strain–displacement matrix in XIGA are obtained as follows:

$$\boldsymbol{B_i^a} = \begin{bmatrix} (R_i)_{,x_1} H & 0 \\ 0 & (R_i)_{,x_2} H \\ (R_i)_{,x_2} H & (R_i)_{,x_1} H \end{bmatrix} \tag{40}$$

$$\boldsymbol{B_i^b} = \begin{bmatrix} B_i^{\mathrm{b}_1} & B_i^{\mathrm{b}_2} & B_i^{\mathrm{b}_3} & B_i^{\mathrm{b}_4} \end{bmatrix} \tag{41}$$

$$\boldsymbol{B_i^{b_\alpha}} = \begin{bmatrix} (R_i S_\alpha)_{,x_1} & 0 \\ 0 & (R_i S_\alpha)_{,x_2} \\ (R_i S_\alpha)_{,x_2} & (R_i S_\alpha)_{,x_1} \end{bmatrix} \tag{42}$$

Where, α= *1, 2, 3, 4*. Finally, the stress and strain components are determined from the displacement approximation, as follows:

$$[\varepsilon] = [B]\{d\} \tag{43}$$

$$[\sigma] = [D][\varepsilon] \tag{44}$$

Where, ε is the strain matrix, {d} is the displacement vector, [σ] is the stress matrix, and [D] is the mechanical properties matrix.

4 THE INTERACTION INTEGRAL METHOD (M-INTEGRAL)

The interaction integral method is derived to investigate Stress Intensity Factors. The interaction integral is obtained from the J-integral. The path-in-dependent J-integral can be expressed as:

$$J = \lim_{n\to\infty} \int_{\Gamma} \left(W\delta_{1j} - \sigma_{ij} u_{i,1}\right) n_j d\Gamma \tag{45}$$

Where, Γ is an arbitrary enclosing contour around the crack tip, δ_{ij} is the Kronecker delta, σ^{ij} are the stress tensor, ε^{ij} are the strain tensor, u_i is the displacement, n_j is the unit outward normal vector perpendicular to the contour Γ, and W is the strain energy density, which is defined as follows:

$$W = \frac{1}{2}\sigma_{ij}\varepsilon_{ij} \tag{46}$$

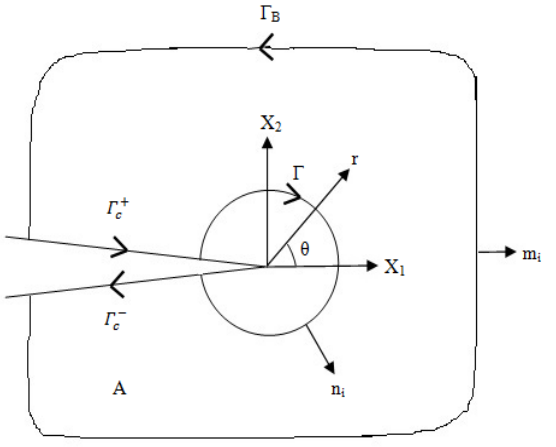

Fig. 7 Contour integrals and domain A is enclosed by Γ_0 and $\Gamma_0 = \Gamma_c^+ + \Gamma + \Gamma_c^- + \Gamma_B$.

Figure 7 Shows the contour of integrals at the crack tip. In the integral interaction method, an auxiliary space is defined and imposed on the main space in the problem. After defining independent spaces, including the actual and auxiliary solution space, the displacements, strains and stresses for both spaces are denoted by (u^{act}, σ^{act},ε^{act}) and (u^{aux}, σ^{aux},ε^{aux}), respectively. The J integral of the superimposed spaces (actual and auxiliary) can be written as [42]:

$$\mathrm{J}^s = \int_\Gamma \left\{\frac{1}{2}(\sigma_{ik}{}^{act} + \sigma_{ik}^{aux})(\varepsilon_{ik}{}^{act} + \varepsilon_{ik}^{aux})\delta_{1j} - (\sigma_{ij}{}^{act} + \sigma_{ij}^{aux})(u_{i,1}{}^{act} + u_{i,1}^{aux})\right\} n_j d\Gamma \quad (47)$$

This integral can be decomposed into:

$$\mathrm{J}^s = \mathrm{J}^{act} + \mathrm{J}^{aux} + M \quad (48)$$

Where, J^{act} is the values of J-integral for the actual state given by "Eq. (45)", J^{aux} is the values of J-integral for the auxiliary state given by:

$$\mathrm{J}^{aux} = \int_\Gamma (W^{aux}\delta_{1j} - \sigma_{ij}^{aux}u_{i,1}^{aux})n_j d\Gamma \quad (49)$$

Where:

$$W^{aux} = \frac{1}{2}\sigma_{ij}^{aux}\varepsilon_{ij}^{aux} \quad (50)$$

And M which is the interaction integral is obtained:

$$\mathrm{M} = \mathrm{J}^s - \mathrm{J}^{act} - \mathrm{J}^{aux} = \int_\Gamma \left[W\delta_{1j} - \sigma_{ij}^{act}u_{i,1}^{aux} - \sigma_{ij}^{aux}u_{i,1}^{act}\right] n_j d\Gamma \quad (51)$$

Where:

$$W = \sigma_{ij}^{act}\varepsilon_{ij}^{aux} = \sigma_{ij}^{aux}\varepsilon_{ij}^{act} \quad (52)$$

The interaction integral is calculated by utilizing stress and strains of the Gaussian integration points in the isogeometric analysis. Note that the integral "Eq. (51)" is not the best suited form for calculations because the integral is on the path. In order to obtain better, more stable and accurate results, the integral on the path can be written in the form of the integral on the surface, thus "Eq. (51)" can be written as:

$$\mathrm{M} = \int_A \left[W\delta_{1j} - \sigma_{ij}^{act}u_{i,1}^{aux} - \sigma_{ij}^{aux}u_{i,1}^{act}\right] q dA \quad (53)$$

Where, A is the interior zone of the arbitrary contour Γ environs the crack tip ("Fig. 8"), and q is a smooth function ranging from $q=0$ on the outer boundary of surface A to $q=1$ on the interior one, as described in "Fig. 9".

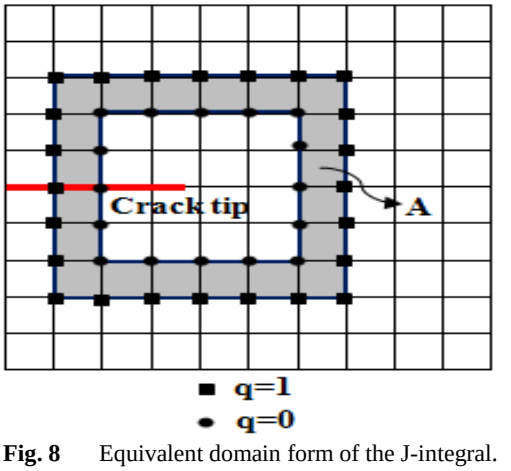

Fig. 8 Equivalent domain form of the J-integral.

In this study, the auxiliary Equations of stress and displacement obtained from William's solution are used [43] to calculate the Stress Intensity Factors in a two-dimensional crack in local Cartesian and polar coordinates, shown in "Fig. 5". These Equations are presented as following forms:

$$\sigma_{ij}^{aux} = \frac{K_I^{aux}}{\sqrt{2\pi r}} f_{ij}^{I}(\theta) + \frac{K_{II}^{aux}}{\sqrt{2\pi r}} f_{ij}^{II}(\theta) \qquad (i,j = 1,2) \tag{54}$$

$$u_i^{aux} = \frac{K_I^{aux}}{\mu}\sqrt{\frac{r}{2\pi}}\, g_i^{I}(\theta) + \frac{K_{II}^{aux}}{\mu}\sqrt{\frac{r}{2\pi}}\, g_i^{II}(\theta) \quad , \quad i,j = 1,2 \tag{55}$$

Where, K_I^{aux} and K_{II}^{aux} are the auxiliary mode I and II stress Intensity Factors, respectively, and μ is the shear modulus at the crack tip, and $f_{ij}(\theta)$ and $g_{ij}(\theta)$ are the angular functions, which are introduced in several Refs [41], [44-45] and expressed by the following forms, respectively:

$$f_{11}^{I}(\theta) = \cos\frac{\theta}{2}\left(1 - \sin\frac{\theta}{2}\sin\frac{3\theta}{2}\right) \tag{56}$$

$$f_{22}^{I}(\theta) = \cos\frac{\theta}{2}\left(1 + \sin\frac{\theta}{2}\sin\frac{3\theta}{2}\right) \tag{57}$$

$$f_{11}^{II}(\theta) = -\sin\frac{\theta}{2}\left(2 + \cos\frac{\theta}{2}\cos\frac{3\theta}{2}\right) \tag{58}$$

$$f_{22}^{II}(\theta) = \sin\frac{\theta}{2}\cos\frac{\theta}{2}\cos\frac{3\theta}{2} \tag{59}$$

$$f_{22}^{II}(\theta) = \sin\frac{\theta}{2}\cos\frac{\theta}{2}\cos\frac{3\theta}{2} \tag{60}$$

$$f_{12}^{I}(\theta) = f_{21}^{I}(\theta) = f_{22}^{II}(\theta)\,, \tag{61}$$

$$f_{12}^{II}(\theta) = f_{21}^{II}(\theta) = f_{22}^{I}(\theta) \tag{62}$$

$$g_1^{I}(\theta) = \frac{1}{4}\left[(2k-1)\cos\frac{\theta}{2} - \cos\frac{3\theta}{2}\right] \tag{63}$$

$$g_2^{I}(\theta) = \frac{1}{4}\left[(2k+1)\sin\frac{\theta}{2} - \sin\frac{3\theta}{2}\right] \tag{64}$$

$$g_1^{II}(\theta) = \frac{1}{4}\left[(2k+3)\sin\frac{\theta}{2} + \sin\frac{3\theta}{2}\right] \tag{65}$$

$$g_2^{II}(\theta) = \frac{1}{4}\left[(2k-3)\cos\frac{\theta}{2} + \cos\frac{3\theta}{2}\right] \tag{66}$$

Where, r and θ are in the polar coordinates, the constant k at the crack tip equals $(3-\vartheta)/(1+\vartheta)$ for plane stress condition, and $(3-4\vartheta)$ for plane strain condition. ϑ is Poisson's ratio. The relationship between J-integral and stress Intensity Factors is expressed as:

$$\mathrm{J} = \frac{K_I^2 + K_{II}^2}{E^*} \tag{67}$$

Where, E^* is given by:

$$E^* = \begin{cases} E & for\ plan\ stress \\ \dfrac{E}{(1-\vartheta^2)} & for\ plane\ strain \end{cases} \tag{68}$$

That is defined in terms of the material parameters, E, Young's modulus, and ϑ, poison's ratio. By substituting actual fields superimposed with auxiliary space into "Eq. (56)" , we obtain:

$$\mathrm{J}^s = \frac{(K_I^{act}{}_I + K_I^{aux})^2 + (K_{II}^{act} + K_{II}^{aux})^2}{E^*} = \mathrm{J}^{act} + \mathrm{J}^{aux} + M \tag{69}$$

Where, J^{aux} is given by:

$$\mathrm{J}^{aux} = \frac{(K_I^{aux})^2 + (K_{II}^{aux})^2}{E^*} \tag{70}$$

Hence, the interaction integral M can be derived:

$$M = \frac{2}{E^*}(K_I^{act}K_I^{aux} + (K_{II}^{act}K_{II}^{aux}) \tag{71}$$

The mode I and II SIFs are decoupled, which are evaluated as below:
For pure mode I will be $K_I^{aux} = 1, K_{II}^{aux} = 0$, correspondingly, Stress Intensity Factors can be derived:

$$K_I^{act} = \frac{E^*}{2} M^{mode\ I} \tag{72}$$

Similarly for pure mode II will be $K_I^{aux} = 0, K_{II}^{aux} = 1$, hence Stress Intensity Factors can be derived:

$$K_{II}^{act} = \frac{E^*}{2} M^{mode\ II} \tag{73}$$

5 FATIGUE CRACK GROWTH ANALYSIS

In linear elastic fracture mechanics, the concept of the stress intensity factor was presented by Paris law to evaluate the stress behavior near the crack tip. The fatigue crack growth rate ($\frac{da}{dN}$) and the stress intensity factor range for cyclic loading (ΔK) can be constituted as a law. The Phrase of Paris law can be written:

$$\frac{da}{dN} = c(\Delta K)^m \tag{74}$$

Where, c and m are Paris low constants parameters. The crack growth simulations are performed subjected to constant amplitude cyclic loading. The range in stress intensity factor (ΔK) for constant amplitude cyclic load is defined as:

$$\Delta K = K_{max} - K_{min} \tag{75}$$

Where, K_{max} and K_{min} are the stress intensity factors corresponding to maximum and minimum applied loads, respectively, after computing crack growth rate, using numerical integration, fatigue life due to the applied cyclic load is calculated.

6 NUMERICAL RESULTS AND DISCUSSION

This section presents several numerical examples of cracks and cracks growth under the assumptions of plane strain two-dimensional elasticity. Cracked plates problems are simulated using XIGA. In order to check the accuracy and performance of XIGA, the results are compared with XFEM. The order of NURBS basic functions in both parametric directions are assumed identical, and to implement K-refinement, they are considered as linear, quadratic, and cubic in different solutions. The values of Stress Intensity Factors are calculated by the interaction integral method. The material properties to solve all the examples are given in "Table 1".

Table 1 Material properties

Elastic modulus, E (GPa)	207
Poisson's ratio, ν	0.3
Fracture toughness, K_{IC} (MPa$\sqrt{m}$)	80
Paris constant, C (m/cycles(MPa$\sqrt{m}$)$^{-m}$)	2.087×10^{-12}
Paris constant, m	3

A plane stress condition is assumed for the modeling. In all examples, a plate of size 200 mm × 400 mm along with an edge cracked and two edges cracked of initial length a_0 = 95 mm and *25* mm, respectively, is taken for the modeling. The plate is subjected to a cyclic tensile load of σ_{min} =0 MPa and σ_{max} =10 MPa at the top edge. The bottom edge of the plate is constrained in the y-direction. A crack growth increment of 1.1 is given at each step of crack growth until the stress intensity factor values (K_I) will be more than the Fracture toughness (K_{IC}). So the new crack length at each step in crack growth is obtained:

$$a_i = 1.1^{i+1}a_0 \tag{76}$$

Where, i is the number of steps of crack growth and a_0 is the initial length of the crack. The stress intensity factor values at each step of crack growth are calculated for evaluating the fatigue life. The geometry and cyclic tensile loads and boundary conditions are shown in "Fig. 9".

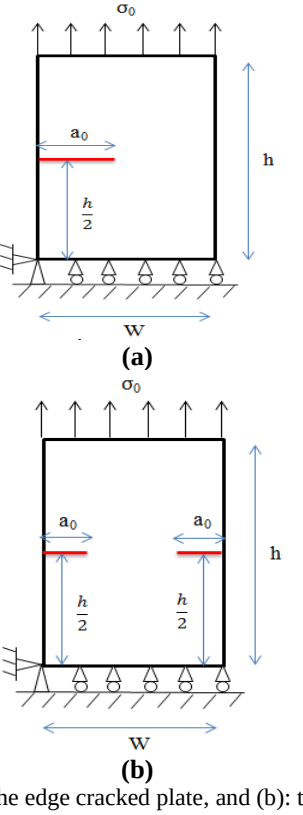

Fig. 9 (a): The edge cracked plate, and (b): the two edges cracked plate.

6.1. Edge cracked plate

With knot vectors and control points, the geometry of the plate is formed. Also, the level set functions; the control points around the crack surface and the crack tip are identified. After calculating the total stiffness matrix, enrichment of control points around the crack surface and the crack tip, applying boundary conditions and force, we obtain displacement and consequently strain and stress values. In order to validate the results of the XIGA method, the problem was solved through the finite element method. Contour plot from the extended isogeometric method and the finite element method are shown in "Fig. 10".

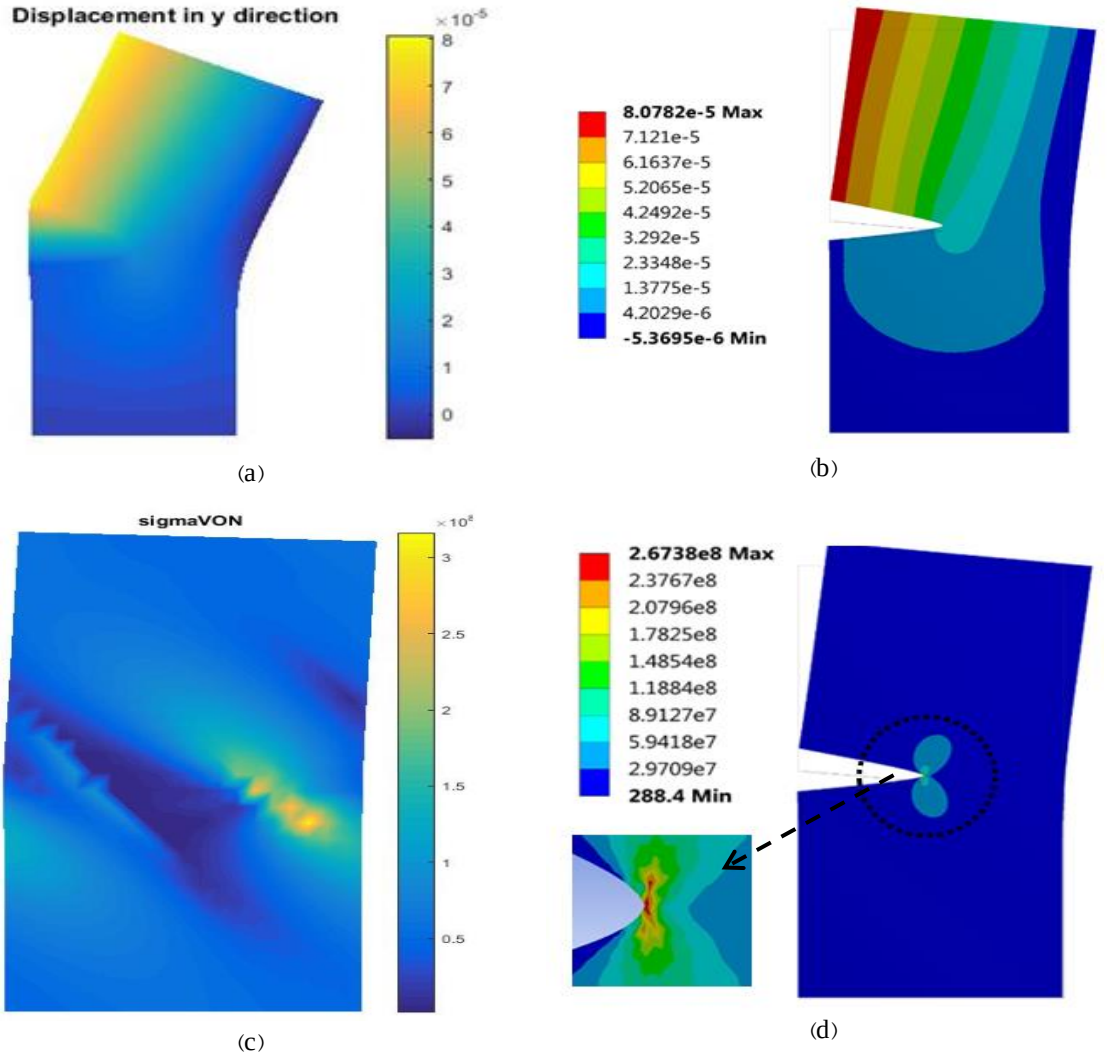

Fig. 10 Comparing the results of XIGA and FEM analysis for edge cracked plate: (a): XIGA displacement in Y direction, (b): FEM displacement in Y direction, (c): XIGA von Mises stress, and (d): FEM von Mises stress.

Maximum displacement in X and Y direction and maximum von Mises stress, obtained by XIGA and FEM are presented in "Table 2". The convergence study and comparison of maximum displacement in X and Y direction obtained by XIGA with linear NURBS basic function and FEM methods are shown in "Fig. 11 and Fig. 12". Compared with FEM, it is observed that the results of XIGA methods converge faster. Convergence is also achieved with fewer elements.

After calculating the displacement and consequently strain and stress values, auxiliary state stress and strain values were derived to calculate stress intensity factor using the interaction integral method. The analytical stress intensity factor for edge cracked plate can be computed as [46]:

$$K_I = \left[1.12 - 0.23\left(\frac{a}{W}\right) + 1.6\left(\frac{a}{W}\right)^2 - 21.7\left(\frac{a}{W}\right)^3 + 30.4\left(\frac{a}{W}\right)^4\right]\sigma\sqrt{\pi a} \quad (77)$$

Where, a is the crack length, and W is plate width. The exact solution is equal to 1.4261×107 (pa√$\boldsymbol{m}$). The results of stress intensity factors obtained by XIGA and FEM methods with linear, quadratic, and cubic NURBS basic functions in the employment of k-refinement are presented in "Table 3". The accuracy of all results is excellent. The stress intensity factor computed using XIGA gives a lower error than FEM. The comparison of values of stress intensity factor of XIGA and FEM is shown in "Fig. 13".

Table 2 Maximum displacement in X and Y direction $\times 10^{-5}$ (m) for edge cracked plate and Maximum von Mises stress $\sigma_{von} \times 10^{7}$ (pa)

FEM				XIGA, (p=q=1)			
No. of elements	U_x^{max}	U_y^{max}	σ_{von}^{max}	No. ofknot span	U_x^{max}	U_y^{max}	σ_{von}^{max}
129	7.2913	7.2957	2.8026	48	7.3356	7.3921	5.9963
191	7.7848	7.6982	4.3082	140	7.7918	7.7267	7.7428
344	8.0084	7.8799	6.4046	600	8.0860	7.9471	9.9254
639	8.1597	8.001	8.1495	1800	8.1838	8.0217	12.185
2356	8.2159	8.0467	12.628	4200	8.2119	8.0435	16.795
42474	8.2551	8.0784	18.144	16200	8.2574	8.0793	25.293
84523	8.2582	8.0806	26.736	25200	8.2608	8.0820	26642

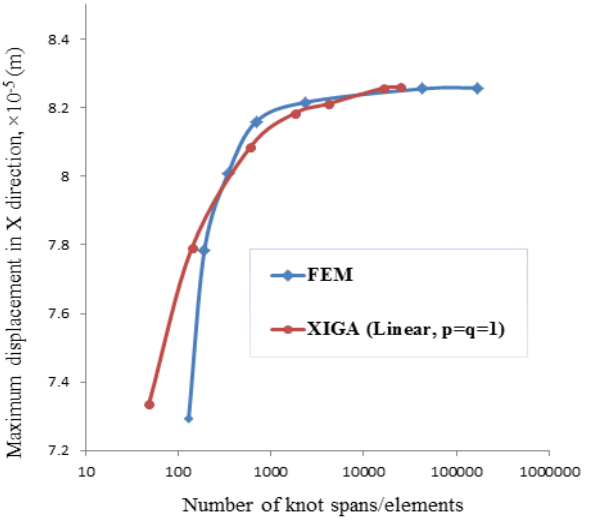

Fig. 11 Convergence study and comparison of maximum displacement in the x-direction for edge cracked plat.

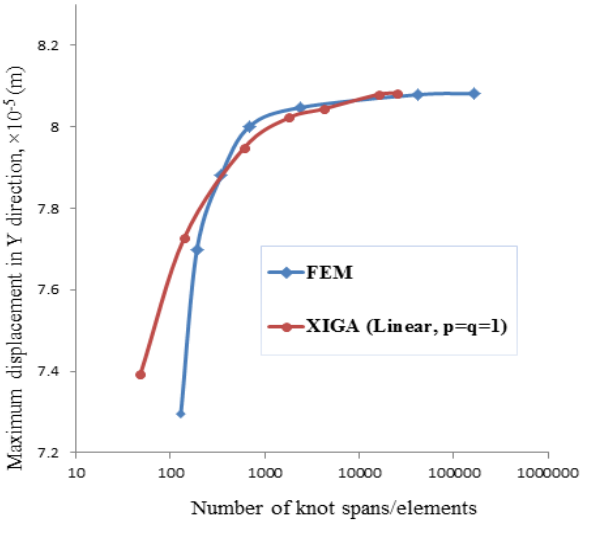

Fig. 12 Convergence study and comparison of maximum displacement in the y-direction for edge cracked plate.

Table 3 Stress intensity factor (K_I), ($pa\sqrt{\boldsymbol{m}}$)$\times 10^7$ to implement K-refinement for edge cracked plate

FEM			XIGA, (p=q=1)			XIGA, (p=q=2)			XIGA, (p=q=3)		
No. of elements	K_I	Error %	No. of knot span	K_I	Error %	No. of knot span	K_I	Error %	No. of knot span	K_I	Error %
129	1.0333	27.54	48	1.2617	11.52	45	1.2498	12.36	44	1.2385	13.15
191	1.3003	8.82	140	1.3707	3.88	70	1.3186	7.54	52	1.2821	10.09
344	1.3604	4.61	600	1.4081	1.54	150	1.3651	4.28	66	1.3523	5.17
639	1.3832	3.01	1800	1.4160	0.63	375	1.4034	1.59	78	1.3698	3.94
2356	1.4059	1.42	4200	1.4194	0.46	750	1.4179	0.87	90	1.3965	2.07
42474	1.4196	0.46	16200	1.4239	0.15	1125	1.4249	0.08	104	1.4264	0.01
84523	1.4235	0.15	25200	1.4254	0.04	1500	1.4257	0.01	-	-	-

The analytical solution is equal to 1.4261

Comparison of stress intensity factor values obtained from the XIGA method with implementing k-refinement is presented in "Fig. 14". It is observed that as NURBS orders are increased, the stress intensity factors converge with fewer elements, and the error is lower compared with the analytical solution. In crack growth simulations, variation of the crack length and calculated values of stress Intensity factor obtained from analytical solution, FEM and XIGA with quadratic NURBS basic function are presented in "Table 4".

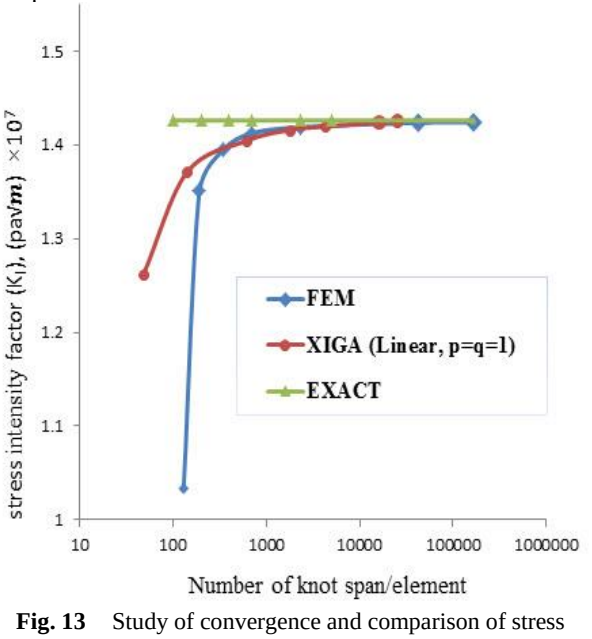

Fig. 13 Study of convergence and comparison of stress intensity factor (K_I) for edge cracked plate.

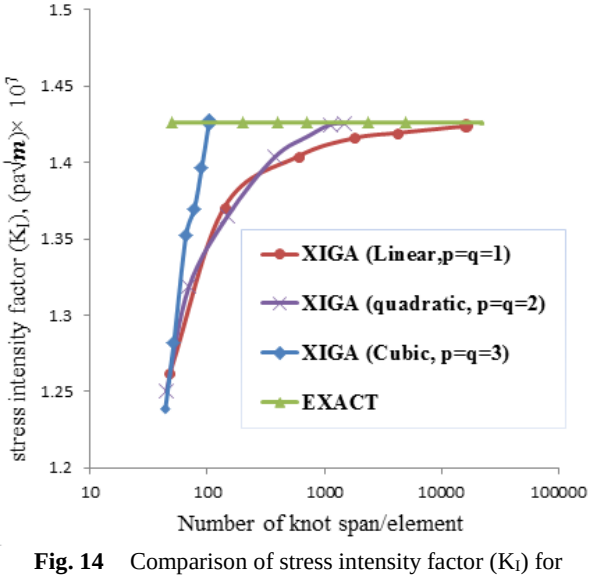

Fig. 14 Comparison of stress intensity factor (K_I) for several order of NURBS function in K-refinement for edge cracked plate.

Figure 15 represents the variation of stress intensity factors with the crack length in fatigue crack growth. Finally, the fatigue life is evaluated by the XIGA method. The fatigue life values are obtained at each step of crack growth until the material fails. These values are presented in "Table 5" and shown in "Fig. 16". It is observed that as the length of the crack reaches 168.6 mm, the stress intensity factor (K_I) values will be more than the Fracture toughness (K_{IC}), and the material fails. Hence, the final crack length is 168.6 mm, and the fatigue life is equal to 149547 cycles.

Table 4 Stress intensity factor (K_I), ($pa\sqrt{m}$)× 10^7 in crack growth of edge cracked plate

Step of crack growth	crack length(m)	K_I EXAT	K_I XIGA	Error %	K_I FEM	Error %
1	0.095	1.4261	1.4257	0.02	1.4196	0.15
2	0.1045	1.7457	1.7385	0.41	1.7278	1.02
3	0.1149	2.2001	2.2004	0.01	2.1901	0.45
4	0.1264	2.8698	2.8121	0.02	2.7446	4.36
5	0.1390	3.8691	3.7524	3.01	3.5743	7.61
6	0.1529	5.3965	5.2314	3.05	5.0211	6.95
7	**0.1686**	**7.8303**	**7.5230**	**3.92**	**7.3915**	**5.60**
8	0.1851	11.455	11.1543	2.62	11.0166	3.82

Table 5 Fatigue life in crack growth for edge cracked plate

Step of crack growth	crack length (m)	Fatigue life (cycle)
1	0.095	36105
2	0.1045	66145
3	0.1149	92451
4	0.1264	115874
5	0.1390	132457
6	0.1529	141863
7	**0.1686**	**149547**

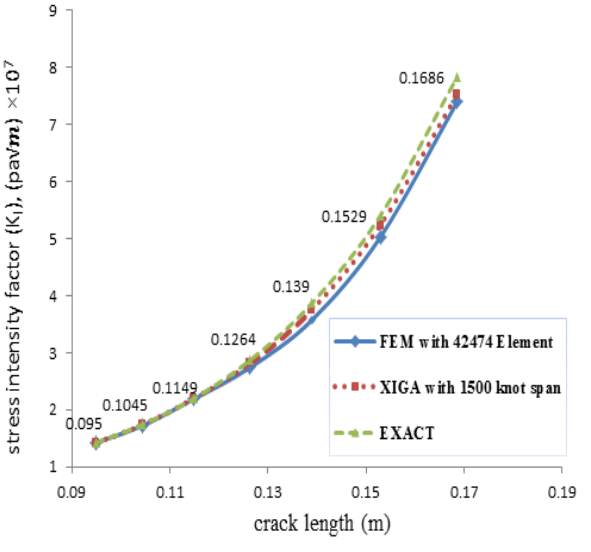

Fig. 15 Comparison of stress intensity factor (K_I) for different crack lengths in crack growth of edge cracked plate.

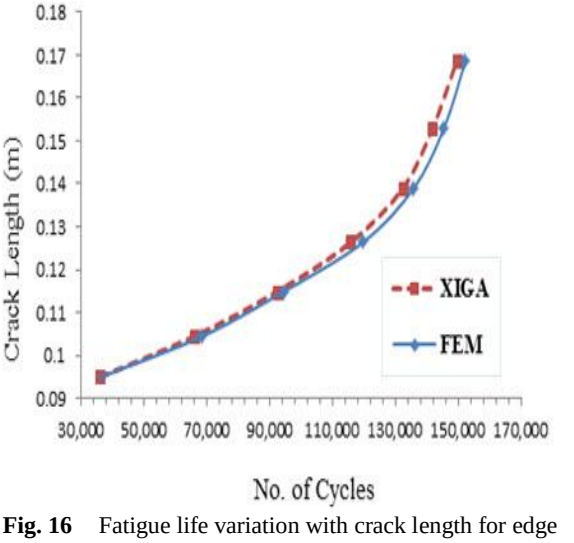

Fig. 16 Fatigue life variation with crack length for edge cracked plate.

6.2. Two Edge Cracked Plate

In this section, a plate with two edges cracked was modeled. the geometry and cyclic tensile loads and boundary conditions are shown in "Fig. 9(b)". Also, Material properties are given in "Table 1". With knot vectors and control points, the geometry of the plate is formed. Also, the level set functions; the control points around the crack surface and the crack tip are identified. After calculating the total stiffness matrix, enrichment of control points around the crack surface and the crack tip, applying boundary conditions and force, we obtain displacement and consequently strain and stress values. To validate the results of the XIGA method, the problem was solved through the finite element method. Contour plot resulted from the extended isogeometric and finite element methods are shown in "Fig. 17".

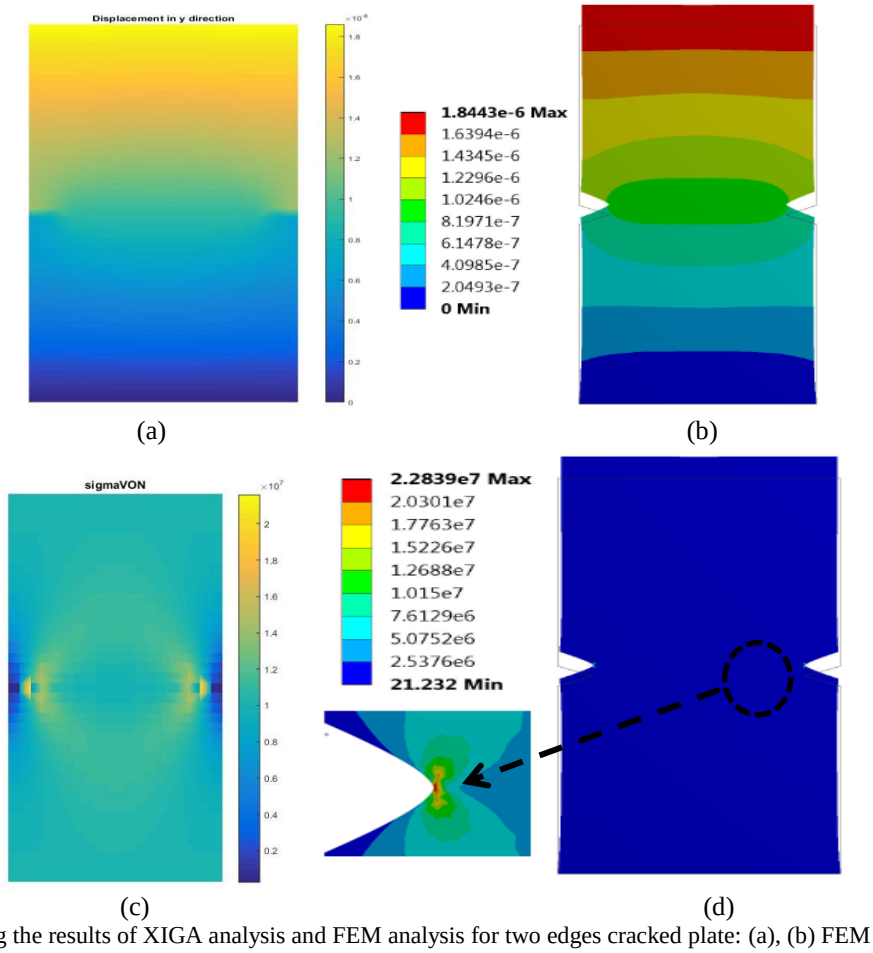

Fig. 17 Comparing the results of XIGA analysis and FEM analysis for two edges cracked plate: (a), (b) FEM displacement in Y direction, (c): XIGA von Mises stress, and (d): FEM von Mises stress.

Maximum displacement in X and Y direction and maximum von Mises stress, obtained by XIGA and FEM are presented in "Table 6".

Table 6 Maximum displacement in X and Y direction $\times 10^{-6}$ `(m) and Maximum von Mises stress $\sigma_{von} \times 10^{7}$ (pa) for two edges cracked plate

FEM				XIGA, (p=q=1)			
No. of elements	U_x^{max}	U_y^{max}	σ_{von}^{max}	No. of knot span	U_x^{max}	U_y^{max}	σ_{von}^{max}
254	2.1506	1.7055	0.4597	42	2.1456	1.70163	0.6891
538	2.1226	1.8098	0.6463	112	2.1244	1.80315	0.8543
1024	2.102	1.8255	0.9422	580	2.1036	1.83169	1.2680
1650	2.0954	1.8335	1.4571	962	2.0912	1.83741	1.6987
2884	2.0897	1.8395	1.8264	1242	2.08854	1.83981	1.9654
45686	2.0909	1.8443	1.893	6420	2.0914	1.84363	2.1256
66888	2.0914	1.8447	2.2839	14600	2.09142	1.84469	2.3265

The convergence study and comparison of maximum displacement in X and Y direction obtained by XIGA with linear NURBS basic function and FEM methods are shown in "Fig. 18" and "Fig. 19". Compared with FEM, it is observed that the results of XIGA methods converge faster. Convergence is also achieved with fewer elements.

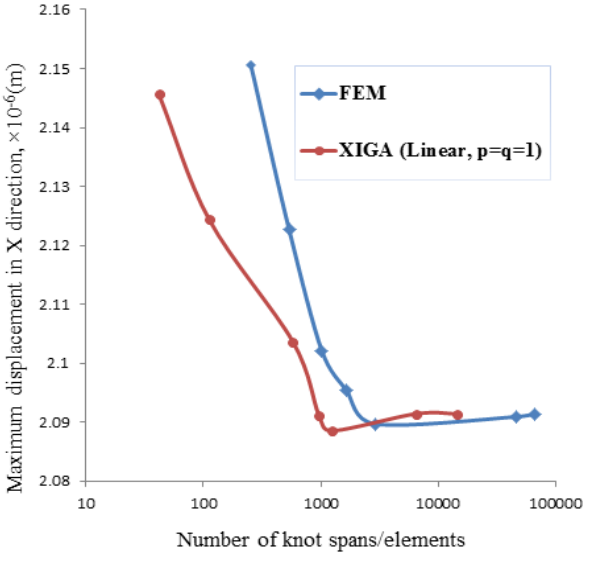

Fig. 18 Convergence study and comparison of maximum displacement in the x-direction for two edges cracked plate.

After calculating the displacement and consequently strain and stress values, auxiliary state stress and strain values are calculated to obtain stress intensity factor using the interaction integral method. The analytical stress intensity factor for two edges cracked plate can be computed as [46]:

$$K_I = \left[1.12 - 0.43\left(\frac{a}{W}\right) + 4.79 - 15.46\left(\frac{a}{W}\right)^3\right]\sigma\sqrt{\pi a} \quad (78)$$

Where, a is the crack length, and W is plate width. The exact solution is equal to 3.1643×10^7 (pa$\sqrt{\boldsymbol{m}}$).

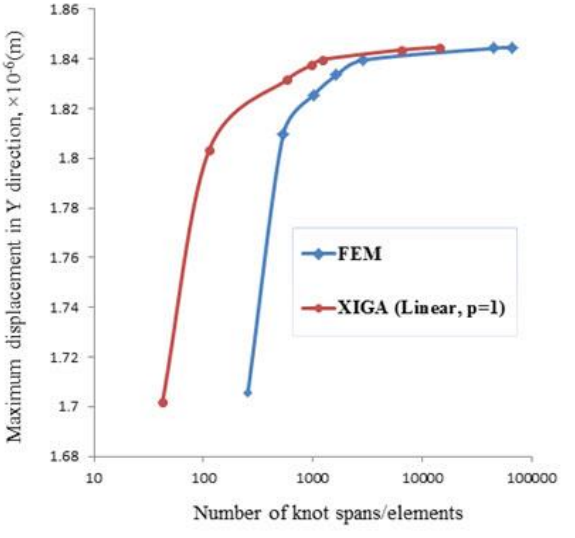

Fig. 19 Convergence study and comparison of maximum displacement in y-direction for two edges cracked plate.

The results of stress intensity factors obtained by XIGA and FEM methods with linear, quadratic, and cubic NURBS basic functions in the employment of k-refinement, are presented in "Table 7".

Table 7 Stress intensity factor (K_I), (pa$\sqrt{\boldsymbol{m}}$)$\times 10^7$ to implement K-refinement for two edge cracked plate

FEM			XIGA, (p=q=1)			XIGA, (p=q=2)			XIGA, (p=q=3)		
No. of elements	K	Error %	No. of knot span	K	Error %	No. of knot span	K	Error %	No. of knot span	K	Error %
254	2.8621	9.55	42	2.9650	6.29	36	2.9841	5.69	25	3.0198	4.56
538	2.9123	7.96	112	3.0228	4.47	64	3.0687	3.02	36	3.1168	1.50
1024	3.0165	4.67	580	3.0874	2.43	100	3.10154	1.98	49	3.1346	0.93
1650	3.0848	2.51	962	3.1098	1.72	225	3.1429	0.67	64	3.1584	0.18
2884	3.1254	1.22	1242	3.1369	0.86	625	3.1547	0.30	81	3.1623	0.06
45686	3.1514	0.4	6420	3.1601	0.13	900	3.1601	0.13	100	3.1645	0.003
66888	3.1612	0.09	14600	3.1627	0.05	1089	3.1637	0.01	-	-	-
The analytical solution is equal to 3.1643											

The accuracy of all results is excellent. The stress intensity factor computed using XIGA gives less error than FEM. Comparison of values of stress intensity factor obtained from XIGA method with implementing k-refinement is shown in "Fig. 20".

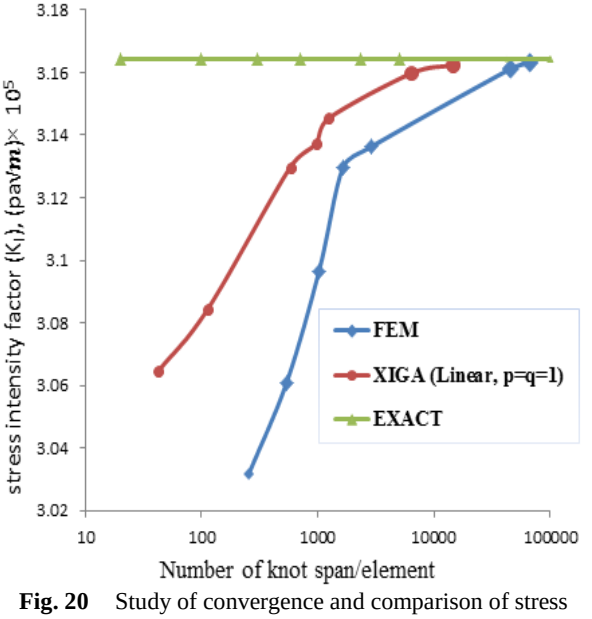

Fig. 20 Study of convergence and comparison of stress intensity factor (K_I) for two edges cracked plate.

The values of stress intensity factor from solving with the XIGA method with K-refinement are presented in "Fig. 21". It is observed that as NURBS orders are increased, the stress intensity factors are convergent with fewer elements, and the error has a smaller value compared with the analytical solution.

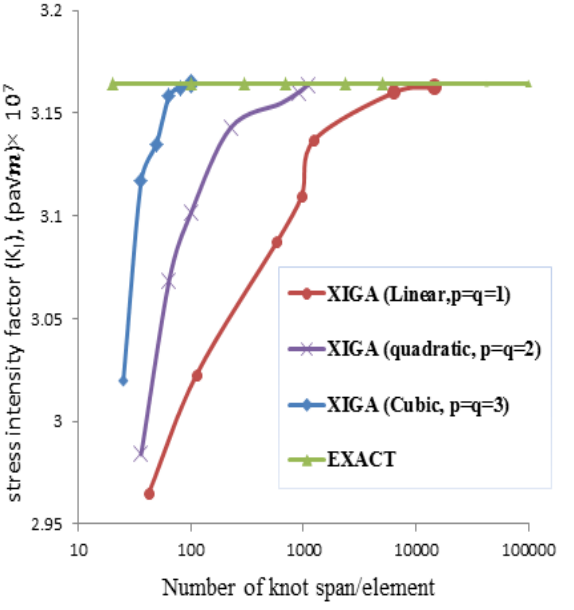

Fig. 21 Comparison of stress intensity factor (K_I) for several order of NURBS function in K-refinement for two edge cracked plate.

In crack growth simulations, variation of the crack length and calculated values of stress intensity factor obtained from analytical solution, FEM, and XIGA with quadratic NURBS basic function are presented in "Table 8".

Table 8 stress intensity factor (K_I) ($pa\sqrt{m}$)× 10^7 crack growth of two edges cracked plate

Step of crack growth	crack length(m)	K_I EXAT	K_I XIGA	Error %	K_I FEM	Error %
1	0.025	3.1643	3.1637	0.01	3.1612	0.09
2	0.0275	3.3171	3.3056	0.34	3.3014	0.47
3	0.03025	3.4803	3.4865	0.17	3.3685	3.21
4	0.03327	3.6537	3.6532	0.01	3.5354	3.23
5	0.03660	3.6725	3.6624	0.27	3.5841	2.40
6	0.04026	3.9577	3.9125	1.14	3.7984	4.02
7	0.04428	4.2824	4.2723	0.23	4.1547	2.98
8	0.04871	4.5532	4.5436	0.21	4.4268	2.77
9	0.05358	4.8768	4.8752	0.03	4.8641	0.26
10	0.05894	5.2773	5.1925	1.60	5.1874	1.70
11	0.06484	5.7895	5.7784	0.19	5.7548	0.59
12	0.07132	6.4625	6.3682	1.45	6.2544	3.22
13	**0.07846**	**7.3722**	**7.2584**	**1.54**	**7.2487**	**1.67**
14	0.08630	8.6215	8.4648	1.81	8.2586	4.20

Figure 22 represents the variation of stress intensity factor with the crack length.

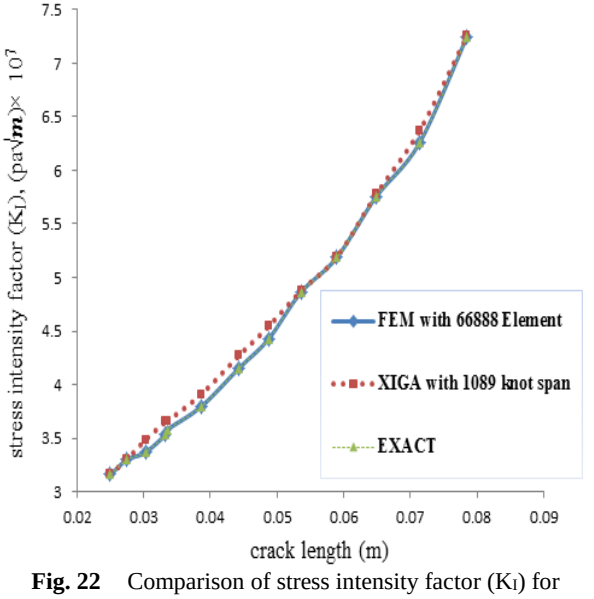

Fig. 22 Comparison of stress intensity factor (K_I) for different crack lengths in crack growth of two edges cracked plate.

Table 9 Fatigue life in crack growth for edge cracked plate

Step of crack growth	crack length (m)	Fatigue life (cycle)
1	0.025	67253
2	0.0275	131657
3	0.03025	190572
4	0.03327	242048
5	0.03660	289642
6	0.03865	329471
7	0.04428	364522
8	0.04871	389654
9	0.05358	407542
10	0.05894	422519
11	0.06484	433178
12	0.07132	441723
13	**0.07846**	**448046**

Finally, the fatigue life is evaluated by the XIGA method. The fatigue life values are obtained at each step of crack growth until the material fails, and they are presented in "Table 9". And shown in "Fig. 23". It is observed that as the length of crack reaches/ is equal to 78.46 mm, the stress intensity factor (K_I) values will be more than the Fracture toughness (K_{IC}), and the material fails. Therefore, the final crack length is 78.46, and fatigue life is equal to 448046 cycles.

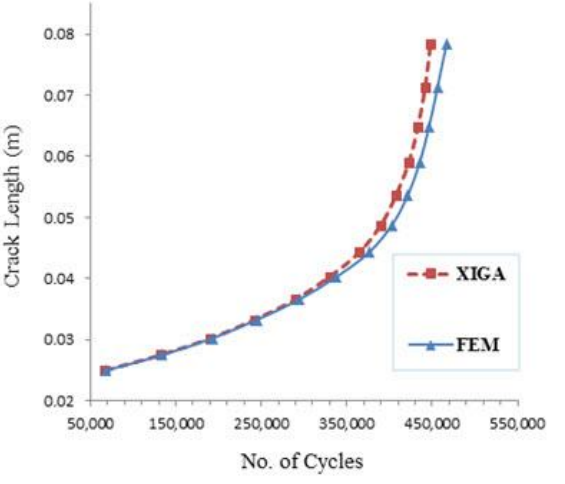

Fig. 23 Fatigue life variation with the crack length for edge cracked plate.

6 CONCLUSIONS

In this research, by a combination of isogeometric analysis with enrichment functions related to crack face and crack tip and employing the level set technique, extended isogeometric analysis formulation is proposed to simulate the cracks in linear elastic fracture mechanic problems. Two different types of enrichment are used for crack face and crack tips. Level set functions are used to identify the knot span related to crack tips and crack face. The fatigue life has been computed using the Paris law of fatigue crack growth. The effect of the k-refinement on the accuracy of the values of stress intensity factor and fatigue life is investigated.

These simulations show that higher accuracy is achieved when using XIGA with higher-order NURBS basic function in k-refinement than using FEM and are closer to the analytical solution results. The best solutions were obtained using k-refinement and it is found that the error is less comparing with the exact solution. It is shown that the efficiency of XIGA with k-refinement is improved. The results confirm the accuracy of the presented XIGA method and its included technique, k-refinement. It is remarkable that this method even requires fewer DOFs than the FEM method. Consequently, XIGA with the k-refinement approach can be used as an alternative in the case of solving linear elastic fracture mechanic problems.

REFERENCES

[1] Nguyen-Xuan, H., Liu, G., Bordas, S., Natarajan, S., and Rabczuk, T., An Adaptive Singular ES-FEM for Mechanics Problems with Singular Field of Arbitrary Order, Computer Methods in Applied Mechanics and Engineering, Vol. 253, 2013, pp. 252-273.

[2] Yan, X., A Boundary Element Modeling of Fatigue Crack Growth in A Plane Elastic Plate, Mechanics Research Communications, Vol. 33, No. 4, 2006, pp. 470-481.

[3] Chen, J. W., Zhou, X. P., The Enhanced Extended Finite Element Method for the Propagation of Complex Branched Cracks, Engineering Analysis with Boundary Elements, Vol. 104, 2019, pp. 46-62.

[4] Xin, H., Veljkovic, M., Fatigue crack Initiation Prediction Using Phantom Nodes-Based Extended Finite Element Method for S355 and S690 Steel Grades, Engineering Fracture Mechanics, Vol. 214, 2019, pp. 164-176.

[5] Hou, J., Zuo, H., Li, Q., Jiang, R., and Zhao, L., Mintegral Analysis For Cracks in a Viscoplastic Material with Extended Finite Element Method, Engineering Fracture Mechanics, Vol. 200, 2018, pp. 294-311.

[6] Apprich, C., Höllig, K., Hörner, J., and Reif, U., Collocation with WEB–Splines, Advances in Computational Mathematics, Vol. 42, No. 4, 2016, pp. 823-842.

[7] Muthu, N., Maiti, S., Yan, W., and Falzon, B., Modelling Interacting Cracks Through a Level Set Using the Element-Free Galerkin Method, International Journal of Mechanical Sciences, Vol. 134, 2017, pp. 203-215.

[8] Hughes, T. J., Cottrell, J. A., and Bazilevs, Y., Isogeometric Analysis: CAD, Finite Elements, Nurbs, Exact Geometry and Mesh Refinement, Computer Methods in Applied Mechanics and Engineering, Vol. 194, No. 39, 2005, pp. 4135-4195.

[9] Belytschko, T., Black, T., Elastic Crack Growth in Finite Elements with Minimal Remeshing, International Journal for Numerical Methods in Engineering, Vol. 45, No. 5, 1999, pp. 601-620.

[10] Moës, N., Dolbow, J., and Belytschko, T., A Finite Element Method for Crack Growth Without Remeshing, International Journal for Numerical Methods in Engineering, Vol. 46, No. 1, 1999, pp. 131-150.

[11] Baietto, M. C., Pierres, E., Gravouil, A., Berthel, B., Fouvry, S., and Trolle, B., Fretting Fatigue Crack Growth Simulation Based on a Combined Experimental and XFEM Strategy, International Journal of Fatigue, Vol. 47, 2013, pp. 31-43.

[12] Stolarska, M., Chopp, D. L., Moës, N., and Belytschko, T., Modelling Crack Growth by Level Sets in the Extended Finite Element Method, International Journal for Numerical Methods in Engineering, Vol. 51, No. 8, 2001, pp. 943-960.

[13] Belytschko, T., Chen, H., Singular Enrichment Finite Element Method for Elastodynamic Crack Propagation, International Journal of Computational Methods, Vol. 1, No. 01, 2004, pp. 1-15.

[14] Ghorashi, S. S., Valizadeh, N., Mohammadi, S., and Rabczuk, T., T-spline Based XIGA for Fracture Analysis of Orthotropic Media, Computers & Structures, Vol. 147, 2015, pp. 138-146.

[15] Gu, J., Yu, T., Nguyen, T. T., Yang, Y., and Bui, T. Q., Fracture Modeling with the Adaptive Xiga Based on Locally Refined B-Splines, Computer Methods in Applied Mechanics and Engineering, Vol. 354, 2019, pp. 527-567.

[16] Peng, X., Atroshchenko, E., Kerfriden, P., and Bordas, S., Isogeometric Boundary Element Methods for Three Dimensional Static Fracture and Fatigue Crack Growth, Computer Methods in Applied Mechanics and Engineering, Vol. 316, 2017, pp. 151-185.

[17] Kumar, S., Singh, I., and Mishra, B., A Coupled Finite Element and Element-Free Galerkin Approach for The Simulation of Stable Crack Growth in Ductile Materials, Theoretical and Applied Fracture Mechanics, Vol. 70, 2014, pp. 49-58.

[18] Shedbale, A., Singh, I., and Mishra, B., A Coupled Fe–EFG Approach for Modelling Crack Growth in Ductile Materials, Fatigue & Fracture of Engineering Materials & Structures, Vol. 39, No. 10, 2016, pp. 1204-1225.

[19] Shedbale, A., Singh, I., Mishra, B., and Sharma, K., Ductile Failure Modeling and Simulations Using Coupled FE–EFG Approach, International Journal of Fracture, Vol. 203, No. 1-2, 2017, pp. 183-209.

[20] Shedbale, A., Singh, I., Mishra, B., and Sharma, K., Evaluation of Mechanical Properties Using Spherical Ball Indentation and Coupled Finite Element–Element-Free Galerkin Approach, Mechanics of Advanced Materials and Structures, Vol. 23, No. 7, 2016, pp. 832-843.

[21] Singh, I., Mishra, B., Bhattacharya, S., and Patil, R., The Numerical Simulation of Fatigue Crack Growth Using Extended Finite Element Method, International Journal of Fatigue, Vol. 36, No. 1, 2012, pp. 109-119.

[22] Kumar, S., Shedbale, A., Singh, I., and Mishra, B., Elasto-Plastic Fatigue Crack Growth Analysis of Plane Problems in The Presence of Flaws Using XFEM, Frontiers of Structural and Civil Engineering, Vol. 9, No. 4, 2015, pp. 420-440.

[23] Menouillard, T., Belytschko, T., Dynamic Fracture with Meshfree Enriched XFEM, Acta Mechanica, Vol. 213, No. 1-2, 2010, pp. 53-69.

[24] Tanaka, S., Suzuki, H., Sadamoto, S., Imachi, M., and Bui, T. Q., Analysis of Cracked Shear Deformable Plates by an Effective Meshfree Plate Formulation, Engineering Fracture Mechanics, Vol. 144, 2015, pp. 142-157.

[25] Tanaka, S., Suzuki, H., Sadamoto, S., Okazawa, S., Yu, T., and Bui, T., Accurate Evaluation of Mixed-Mode Intensity Factors of Cracked Shear-Deformable Plates by an Enriched Meshfree Galerkin Formulation, Archive of Applied Mechanics, Vol. 87, No. 2, 2017, pp. 279-298.

[26] Tran, L. V., Ferreira, A., and Nguyen-Xuan, H., Isogeometric Analysis of Functionally Graded Plates Using Higher-Order Shear Deformation Theory, Composites Part B: Engineering, Vol. 51, 2013, pp. 368-383.

[27] Yuan, H., Liu, W., and Xie, Y., Mode-I Stress Intensity Factors for Cracked Special-Shaped Shells Under Bending, Engineering Fracture Mechanics, Vol. 207, 2019, pp. 131-148.

[28] Nguyen, B., Tran, H., Anitescu, C., Zhuang, X., and Rabczuk, T., An Isogeometric Symmetric Galerkin Boundary Element Method for Two-Dimensional Crack Problems, Computer Methods in Applied Mechanics and Engineering, Vol. 306, 2016, pp. 252-275.

[29] Verhoosel, C. V., Scott, M. A., De Borst, R., and Hughes, T. J., An Isogeometric Approach to Cohesive Zone Modeling, International Journal for Numerical Methods in Engineering, Vol. 87, No. 1-5, 2011, pp. 336-360.

[30] Verhoosel, C. V., Scott, M. A., Hughes, T. J., and De Borst, R., An Isogeometric Analysis Approach to Gradient Damage Models, International Journal for Numerical Methods in Engineering, Vol. 86, No. 1, 2011, pp. 115-134.

[31] Hao, P., Yuan, X., Liu, H., Wang, B., Liu, C., Yang, D., and Zhan, S., Isogeometric Buckling Analysis of Composite Variable-Stiffness Panels, Composite Structures, Vol. 165, 2017, pp. 192-208.

[32] Tran, L. V., Ly, H. A., Lee, J., Wahab, M. A., and Nguyen-Xuan, H., Vibration Analysis of Cracked Fgm Plates Using Higher-Order Shear Deformation Theory and Extended Isogeometric Approach, International Journal of Mechanical Sciences, Vol. 96, 2015, pp. 65-78.

[33] Bhardwaj, G., Singh, I., and Mishra, B., Numerical Simulation of Plane Crack Problems Using Extended Isogeometric Analysis, Procedia Engineering, Vol. 64, 2013, pp. 661-670.

[34] Bhardwaj, G., Singh, I., Mishra, B., and Kumar, V., Numerical Simulations of Cracked Plate Using Xiga Under Different Loads and Boundary Conditions, Mechanics of Advanced Materials and Structures, Vol. 23, No. 6, 2016, pp. 704-714.

[35] Nguyen-Thanh, N., Valizadeh, N., Nguyen, M., Nguyen-Xuan, H., Zhuang, X., Areias, P., Zi, G., Bazilevs, Y., De Lorenzis, L., and Rabczuk, T., An Extended Isogeometric Thin Shell Analysis Based on Kirchhoff–Love Theory, Computer Methods in Applied Mechanics and Engineering, Vol. 284, 2015, pp. 265-291.

[36] Singh, A. K., Jameel, A., and Harmain, G., Investigations on Crack Tip Plastic Zones by the Extended Iso-Geometric Analysis, Materials Today: Proceedings, Vol. 5, No. 9, 2018, pp. 19284-19293.

[37] Roh, H. Y., Cho, M., The Application of Geometrically Exact Shell Elements to B-Spline Surfaces, Computer Methods in Applied Mechanics and Engineering, Vol. 193, No. 23-26, 2004, pp. 2261-2299.

[38] Piegl, L., Tiller, W., The NURBS Book, Second Edition, Springer Science & Business Media, Germany, 2012, 3642592236.

[39] Cottrell, J., Hughes, T., and Reali, A., Studies of Refinement and Continuity in Isogeometric Structural Analysis, Computer Methods in Applied Mechanics and Engineering, Vol. 196, No. 41-44, 2007, pp. 4160-4183.

[40] Cottrell, J. A., Hughes, T. J., and Bazilevs, Y., Isogeometric Analysis Toward Integration of CAD and FEA, John Wiley & Sons, United Kingdom, 2009, 0470749091.

[41] Sutradhar, A., Paulino, G. H., Symmetric Galerkin Boundary Element Computation of T-Stress and Stress Intensity Factors for Mixed-Mode Cracks by the Interaction Integral Method, Engineering Analysis with Boundary Elements, Vol. 28, No. 11, 2004, pp. 1335-1350.

[42] Mohammadi, S., Extended Finite Element Method for Fracture Analysis of Structures, John Wiley & Sons, Oxford OX4 2DQ, United Kingdom, 2008, 0470697997.

[43] Williams, M., Gn the Stress Distribution at the Base of a Stationary Crack. I. Appl. 1957, Mech.

[44] Guo, F., Guo, L., Huang, K., Bai, X., Zhong, S., and Yu, H., An Interaction Energy Integral Method for T-Stress Evaluation in Nonhomogeneous Materials Under Thermal Loading, Mechanics of Materials, Vol. 83, 2015, pp. 30-39.

[45] Bremberg, D., Faleskog, J., A Numerical Procedure for Interaction Integrals Developed for Curved Cracks of General Shape in 3-D, International Journal of Solids and Structures, Vol. 62, 2015, pp. 144-157.

[46] Yoon, M., Cho, S., Isogeometric Shape Design Sensitivity Analysis of Elasticity Problems Using Boundary Integral Equations, Engineering Analysis with Boundary Elements, Vol. 66, 2016, pp. 119-128.